Self-assembling of Ge dots on nanopatterns: Experimental investigation of their formation, evolution and control

I. Berbezier and A. Ronda

L2MP, CNRS, Univ. Paul Cézanne, Avenue Escadrille Normandie Niemen – Case 142, 13397 Marseille Cedex 20, France

(Received 6 April 2006; revised manuscript received 26 October 2006; published 4 May 2007)

Understanding and predicting quantum dots ordering is a central problem for many physical processes. Here, we investigate the mechanisms which govern the self-assembling of Ge dots on nanopatterned vicinal Si substrate. In a first part, we investigate the formation of nanopatterns by self-organization of growth instabilities which develop during epitaxial growth of Si and $Si_{1-x}Ge_x$ layers on Si substrates. Evolution laws of kinetic and thermodynamic growth instabilities as a function of temperature, deposited thickness, and strain are determined on vicinal (111) and (001). In a second part, we analyze the Ge dots ordering on full scale wafer patterns formed by self-organization of the growth instabilities. Depending on the nature of the latter ones, we show that Ge dots can align either in the valley of the instability undulations or on their top. We explain these results by the predominant effect of surface diffusion, surface free energy anisotropy, and strain energy relaxation, respectively.

DOI: 10.1103/PhysRevB.75.195407 PACS number(s): 81.16.Rf, 61.46.Hk, 81.07.Ta, 68.37.−d

I. INTRODUCTION

Spontaneous self-organization of periodic nanostructures has been studied extensively during the past years, mainly because of their possible applications in nanoscale devices. It is commonly suggested that the main mechanism of the formation of quantum dots is the Stranski-Krastanov growth mode.[1–3] It is shown that nucleation of Ge dots on nominal Si(001) is mainly random without preferential nucleation sites.[4,5] It has been reported that growth instabilities can be used as nanotemplates or nanopatterns, in particular, kinetic (step-bunching and step-meandering) and thermodynamic (step-bunching, faceting, and stress-driven) instabilities were suggested as a means to self-organize regular patterns.[6] To exploit these mechanisms, a fundamental control and understanding of the instability behavior is required.

A first issue is to create nanopatterns using growth instabilities. The step bunching instability that occurs during growth has been explained by the presence of contaminants,[7] by anisotropy of surface diffusion,[8,9] or by an inverse Schwoebel barrier.[10,11] With deposition time, step-bunches self-organize up to the formation of regular arrays of periodic undulations with specific features.[12–14] A combination of step bunching and step meandering could also induce the formation of quantum dots.[15,16] Other mechanisms can also play an important role in the formation of quantum dots. For example, a faceting of a thermodynamically unstable surface caused by surface energy anisotropy can produce, in certain conditions, a stable periodic array of quantum dots.[17] In particular, the formation of self-organized patterns has been demonstrated on Si(111) surfaces miscut in the [−211] direction.[18]

Moreover, growth instabilities that develop during epitaxy of $Si_{1-x}Ge_x$ on silicon substrates also produce highly corrugated periodic and reproducible patterns on a full scale wafer[19–26] that could be efficiently used as templates for subsequent ordering of Ge islands[27–31] without the need of sophisticated lithographic tools. Several theoretical models have been developed to describe the stress-driven growth instability.[32–39] They have allowed one to qualitatively and quantitatively explain most of the experimental results. Several basic issues concerning the physical mechanisms involved in the different stages of the formation and evolution of islands are only becoming clear these last years. For instance, the morphological evolution of the instability with substrate crystallographic orientation[40] and the opposite effect of stresses of opposite sign[41] were attributed recently to the strain dependence of the step energy[42] and of the facet energy.[43] However, the critical exponents of instability self-organization and growth reported in the literature still differ from one model to another depending on the mass transport and atomistic parameters considered in addition to the classical stress/capillarity energy balance of elasticity theory.

A second issue concerns the Ge dots self-assembling on patterned substrates. Despite the large number of studies reported in the literature, the physical mechanisms of nucleation and evolution of three-dimensional (3D) Ge dots are still under debate. In particular, various island nucleation processes have been identified by STM observations: random nucleation,[5,44] preferential nucleation at step edges on Si(111),[45] nucleation in between dimmer vacancy lines,[46] barrier less formation from surface ripples,[47,48] or from a Ge-induced faceting transition[49] on vicinal substrates. Up to now the relative roles of stress, surface energy anisotropy, and surface diffusion have not been clearly established experimentally. Nevertheless, it has been shown that Ge islands preferentially nucleate along the edges of mesas[50] and on dislocation lines.[51] These results were explained by the main effect of stress gradients on island nucleation. However, another driving force, such as surface free energy anisotropy, was also suggested to explain the preferential nucleation along the mesas edges.[31]

The focus of this work is to understand the experimental conditions (growth temperature, substrate crystalline orientation, misorientation, and strain) on the formation and self-organization of growth instabilities. We then investigate the influence of specific patterns on Ge dots self-assembling processes. In particular, we focus on the effect of step bunches,

 ©2007 The American Physical Society

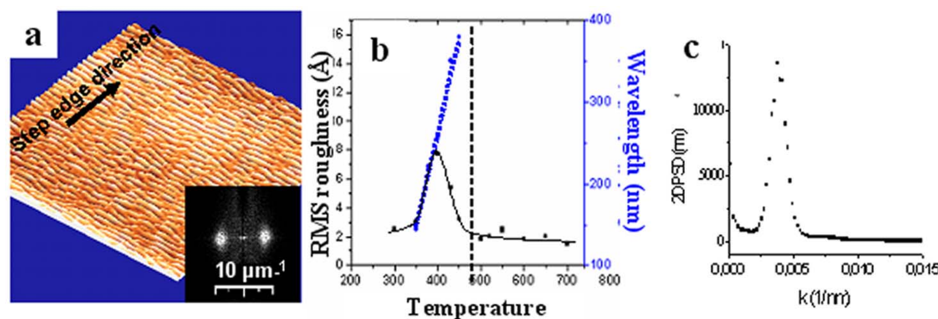

FIG. 1. (Color online) Characteristics of the step bunching instability which develops during deposition of Si on Si (001) 1.5° off. (a) AFM image (scan size 5×5 μm^2) of 500 nm Si deposited at T_g=450 °C. The mean height of the periodic ripples is ~3.5 nm. The inset shows the 2D Fourier transform of the image. (b) Evolution of rms roughness and wavelength with T_g. (c) 2D power spectrum density of AFM image 5×5 μm^2

nano-facets, and compressive strain on self-assembling processes. The results evidence the preferential nucleation of Ge dots either inside the valley (along the step bunches or at the intersection between the nanofacets) or on the top of the undulations. We explain these results by the respective effects of surface diffusion, surface energy anisotropy, and strain relaxation. We show that remarkable Ge dots ordering can be obtained on self-organized growth instability without the need of lithographic patterning.

II. EXPERIMENT

The samples were grown in a Riber molecular beam epitaxy (MBE) chamber with a base pressure in the 10^{-11} torr range. Si and Ge were evaporated from an electron beam evaporator and an effusion cell, respectively. The deposition rate of Si was maintained constant at about 0.03 nm/s. $Si_{1-x}Ge_x$ alloyed layers with x comprised between 0 and 0.5 were deposited either on nominal or on vicinal (001) and (111) surfaces. Vicinal (001) and (111) surfaces were misoriented in the [110] and the [−1−12] or [11−2] direction, respectively, with a miscut angle, θ, varying between 0° and 10°. *In situ* cleaning of the substrate consisted of a two-temperature process (830 °C/30 min and 1230 °C/2 min), which resulted in a sharp 2D reflection high-energy electron diffraction (RHEED) pattern, indicative of a clean surface. Prior to the growth of the $Si_{1-x}Ge_x$ layers, a 50-nm thick Si buffer layer was systematically grown at 750 °C to achieve a reproducible flat surface. Morphological characterization of the samples was performed by atomic force microscopy (AFM) operating in air and by transmission electron microscopy (TEM) cross-section observations.

For the self-assembling of Ge dots experiments a two step growth process was used: the deposition of the self-organized template layer followed by the subsequent deposition of 8 ML of Ge at a growth temperature, $T_G\sim600$ °C after a short growth interruption ($t\sim10$ min).

III. RESULTS

A. Formation of nanopatterns

In this part we investigate the formation and self-organization of a periodic corrugation that develops during the growth of Si and $Si_{1-x}Ge_x$ on vicinal Si substrates. It is necessary to determine the evolution of nanopatterns periodicity, amplitude, and shape with experimental parameters in order to optimize the subsequent ordering of Ge dots.

First, we consider the epitaxy of Si/Si (001) vicinal substrates (i.e., growth without stress). It was reported that step bunching instability develops on Si substrates at a critical temperature.[13,52] Such instability gives rise to nice periodic undulations perpendicular to the miscut direction (i.e., parallel to the step edges) for all the miscut angles investigated ($1.5°<\theta<10°$). Periodicity of the patterns (~250 nm on the example presented) can be well-appreciated on the AFM image and on the 2D fast Fourier transform (FFT) [Fig. 1(a)]. A correlation length of ~1 μm is extracted from the quantitative analysis of the 2D power spectral density (PSD) presented in Fig. 1(c). A systematic investigation of amplitude (A) and wavelength (λ) as a function of growth temperature (T_g) and deposited thickness (h) was performed. Results evidence a very narrow temperature regime of the instability, which coincides with the transition between 2D islands nucleation and step flow growth modes [Fig. 1(b)]. Using kinetic Monte Carlo simulations,[9] we showed that the instability originates from the anisotropy of diffusion barrier induced by the $(2\times1+1\times2)$ surface reconstruction. Similar results were found using a continuum growth model.[8] Morphological evolution of the undulation with time was discussed in detail in Ref. 9.

Second, we investigate the epitaxial growth of Si/Si (111) vicinal with misorientations around [1−10] towards [11−2] and [−1−12] directions. For misorientations towards [11 −2] the starting surface after high temperature flash consists of regular train of monolayer steps separating flat terraces ~1.8 nm wide [Fig. 2(a)], the height of a monolayer step being 3.13 Å in Si(111). Such morphology has already been described in the literature.[53] During Si growth the surface breaks down into a sawtooth morphology [Fig. 2(b)] consisting of (111) and (332) facets [Fig. 2(c)]. This behavior is attributed to a faceting instability which has been well-described in the literature.[17,54,55] The ripples can be better appreciated on the AFM image [Fig. 2(d)]. From the 2DFFT of the Si(111) 1,5° off faceted surface we can see that the size distribution of the ripples is rather broad [inset of Fig. 2(d)]. We can conclude that in our experimental conditions

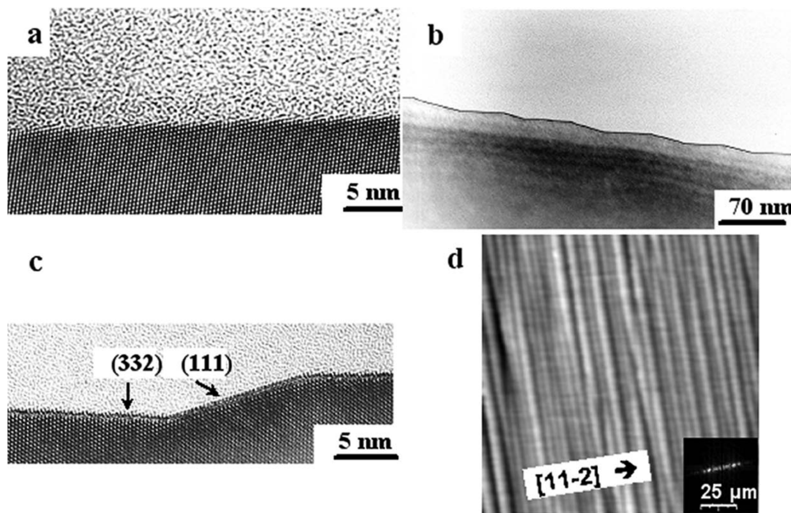

FIG. 2. TEM cross-section images of Si(111) misoriented of 10° off towards [11−2] (a) before growth and (b) after 500 nm Si deposition at 700 °C. (c) At higher magnification, (332) and (111) facets identified by arrows are clearly visible. (d) AFM image of the faceted surface obtained by deposition of 500 nm Si on Si(111) 1.5° off. In the inset is given the 2DFFT of the surface. Gray vertical scale: black to white is 3 nm. Scan size is 3×3 μm^2.

the self-organization of faceting instability leads to a periodic surface with broad size distribution, even if a well-defined periodicity of the sawtooth profile has been predicted and theoretically explained by surface energy and surface stress minimization. The periodicity was expected to be independent of the miscut angle while the width of the (332) facets was linearly decreasing with the miscut angle.[18]

For misorientations towards [−1−12], the starting surface after high temperature flash consists of a regular train of triple-layer steps 9.4 Å high. Figure 3(a) exhibits an example of the triple layer steps for a vicinal substrate misoriented 10°. During Si growth, a periodic step bunching instability develops. An example of the instability developed on Si(111) 1,5° off is presented in Fig. 3(b). We can observe on the surface a periodic alternation of areas with high and low steps density. The period measured from the 2DFFT of the image is 750 nm [inset of Fig. 2(b)]. Such morphology cannot be confused with faceted morphology described above due to the absence of extended facets and to the large scale periodicity evidenced by a correlation length of 1.5 μm. The temperature range of the instability regime is comprised between 650 and 800 °C [Fig. 3(c)] with a maximum of the instability amplitude at ~750 °C. At lower and at higher temperatures, the instability vanishes and growth recovers the normal step flow mode and the surface exhibits a regular train of monoatomic steps. A similar behavior was also observed in the case of substrates misoriented 10° towards [−1−12] but the instability developed at lower temperature (maximum of the instability amplitude at ~700 °C on 10° off instead of 750 °C on 1,5° off). On both misorientations, the instability develops when 7×7 and 1×1 reconstructed areas coexist on the surface, during the gradual vanishing of 7×7 surface reconstruction at the expense of 1×1. Following the same argument than for step bunching instability on vicinal Si(001), we suggest that the size of terraces could fluctuate during growth. In this situation if 7×7 reconstruction is only present on large terraces and not on smaller ones, anisotropy of surface diffusion will be generated between these terraces due to the larger diffusion barrier on 7×7 than on 1×1 reconstructed terraces.[56] Consequently during growth, large terraces will become larger and small terraces will become smaller leading to the step bunching instability. We show that wavelength and amplitude of the instability increase with the deposition time t (or deposited thickness h). These evolutions could be fitted by power laws $\lambda\propto t^{\alpha}$ and $A\propto t^{\beta}$ with critical exponents: $\alpha\sim0.23$ and $\beta\sim0.5$, respectively [Figs. 3(d) and 3(e), respectively].

Third, we describe the self-organization of $Si_{1-x}Ge_x$ instability that develops on misoriented Si(001) substrates. It is well-known that $Si_{1-x}Ge_x$ growth instability is kinetically activated and does not appear at temperatures below 500 °C.[40] Moreover, since the instability is inhibited on a singular Si(111) substrate but appears on vicinal Si(111), it was concluded that it is strongly dependent on the surface energy anisotropy.[23]

Here, we consider the morphological evolution of the instability on vicinal substrates. First we investigate the evolution with the miscut angle. Examples of periodic patterns developed during the growth of 10 nm $Si_{1-x}Ge_x$ (x=0.35) on Si(001) misoriented 1.5° and 10° are presented in Fig. 4. At low miscut angles (<2°), the instability self-organizes into periodic 2D arrays constituted of undulations with rectangular bases aligned along both [010] and [100] at 45° from the step edges [Fig. 4(a)]. This square-based self-organization process is also evidenced by the symmetry 4 observed on 2DFFT with a correlation length of ~1 μm measured from the 2DPSD. Such morphology has been explained by a novel rebonded [100] oriented single-height step stabilized by compressive strain.[42] At larger miscut angles (>8°) the patterns self-organize into periodic 1D wires elongated perpendicular to the step edges with a correlation length of ~0.8 μm [Fig. 4(b)]. STM observations evidence the presence of (105) facets on the sidewalls of the undulation made up by [110] oriented monolayer steps.[57] Such behavior considerably differs from the strain induced step bunching process reported in Ref. 58. Recently, formation of these undulations with sidewalls oriented along (105) facets has been theoretically explained.[46,47] The authors demonstrate that (100) becomes unstable under a compressive mismatch strain, and that its surface energy arrives at a minimum at an orientation around (105). The ripple formation is then considered as a nucleationless process due to the lowering of

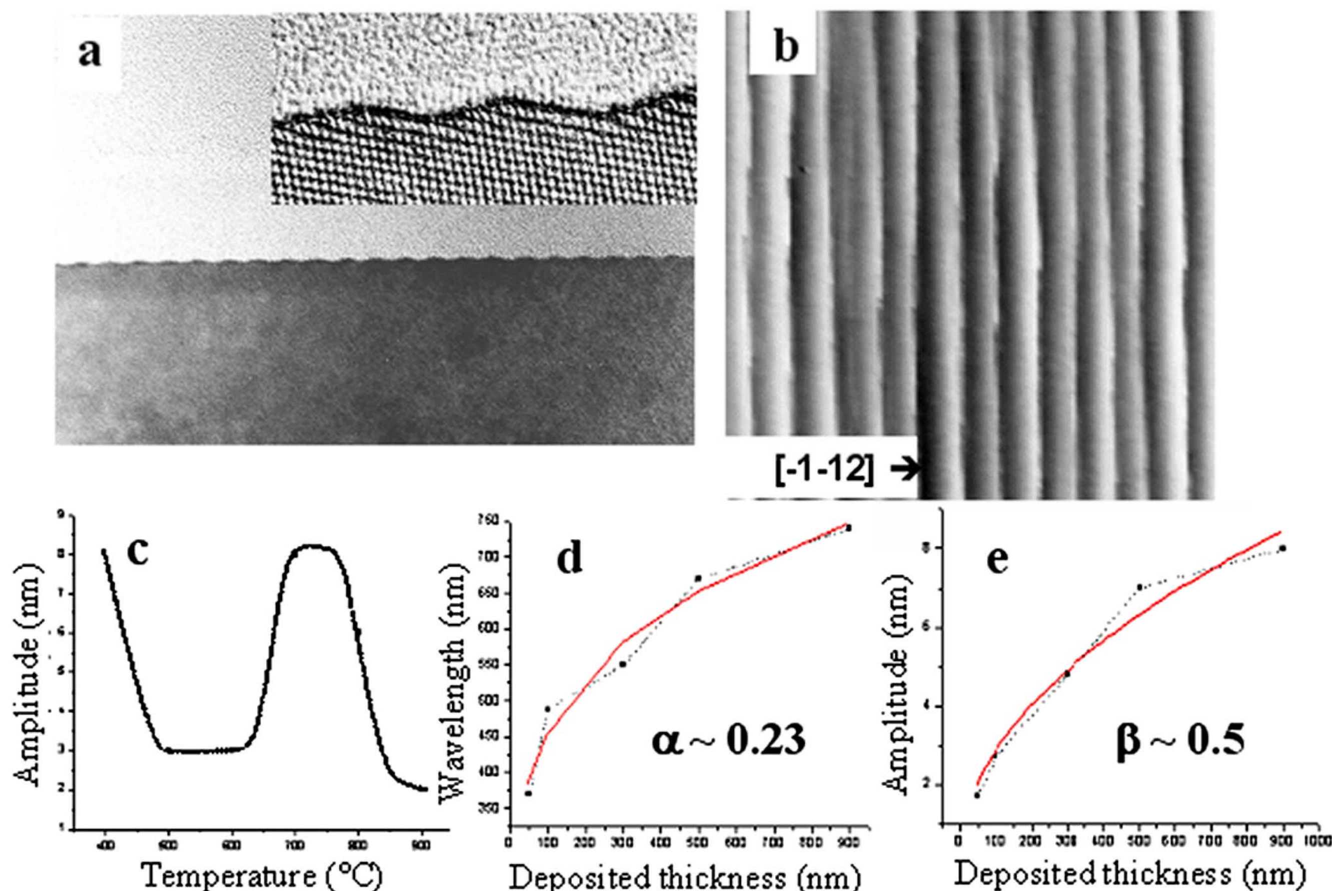

FIG. 3. (Color online) (a) TEM cross-section image of Si (111) 10° off toward [−1−12] before growth. High resolution image of the triple steps is shown in the inset. (b) AFM image of a 500 nm thick Si layer deposited at T_g=750 °C on Si 1.5° off. In the inset is given the 2DFFT of the surface. Gray vertical scale: black to white is 14 nm. Scan size is $10\times10\ \mu m^2$. (c) Temperature dependent evolution of the instability amplitude. (d) and (e) give the wavelength (λ) and amplitude (A) evolution with h (deposited thickness). Continuous lines represent the best fit of the data.

step formation energies under compressive stress. It was also reported that the peculiar surface reconstruction of (105) facets would be responsible for their stability.[59,60] Consequently, formation of 1D wires perpendicular to the step edges could be explained by the minimization of the strain dependent surface energy in agreement with theoretical predictions.[61] This explains why for increasing miscut angles, undulation sides extend perpendicularly to the step edges, while remaining parallel to (105) facets as can be seen on the stereographic projection of a 10° off vicinal substrate [Fig. 4(c)]. Moreover, the anisotropy of instability shape could also be favored by a higher strain relaxation when Ge atoms are located on the step edges.[62]

For all the misorientations tested (θ varying between 0.3° and 10°), the instability wavelength in the perpendicular direction (parallel to the step edges) and the instability amplitude are almost constant (Table I).

We have then investigated the morphological evolution of the instability on vicinal Si(001) 1.5° off. Variations of rms and λ with h (deposited thickness) and x (Ge concentration) are reported in Fig. 5. Regarding the morphological evolution with h we have used $Si_{1-x}Ge_x$ layers with $x\sim0.25$. The results show that the instability onset occurs at a critical thickness $h_0\sim40$ nm. For larger thickness ($40\text{ nm}<h<100$ nm), the instability starts to self-organize and the rms roughness increases linearly with h [Fig. 5(b)] while λ remains constant with the deposition time [Fig. 5(a)]. For larger h (>100 nm), the surface morphology evolution abruptly changes due to the nucleation of misfit dislocations evidenced on AFM images by a cross-hatch pattern (not shown). This growth regime is out of the scope of this paper.

Regarding the instability evolution with x we have used $Si_{1-x}Ge_x$ layers with $h\sim40$ nm and $x<0.3$. The composition range is limited due to the formation of 3D islands and to the nucleation of dislocations, at larger Ge concentrations, which both affect the instability evolution. The results evidenced in Figs. 5(c) and 5(d) show that λ decreases linearly with x, while rms roughness increases linearly with x.

These results prove that the instability evolution on vicinal substrate differs considerably from the one previously reported on nominal Si(001), obtained in similar experimental conditions.[23] In the latter work, evolutions of the instability amplitude $A\propto x^2$, $A\propto h$ and wavelength $\lambda\propto x^{-1}$ were obtained.

$Si_{1-x}Ge_x$ instability presents a very complex evolution induced by the interplay of many experimental parameters

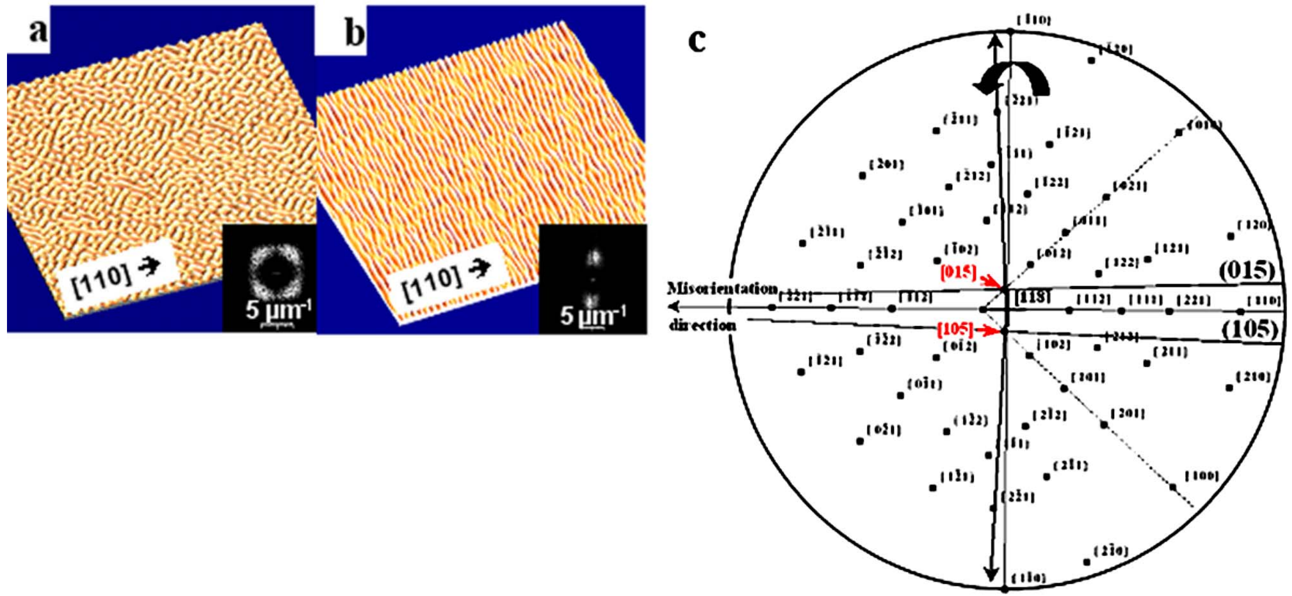

FIG. 4. (Color online) Surface morphology of 10 nm $Si_{1-x}Ge_x$ layers ($x \sim 0.35$) deposited on vicinal Si(001): (a) 1.5° off and (b) 10° off. Scan size is $10\times 10\ \mu m^2$. The mean heights of the ripples are 20 and 9 nm, respectively. 2DFFT are given in the insets. (c) Stereographic projection of (118) surface [which corresponds to Si(001) 10° off].

such as the substrate orientation (both density of steps and substrate stiffness influence the onset and the development of the instability), surface diffusion, growth temperature, deposited thickness, and misfit stress. In order to explain these results, we have analyzed some of the theoretical models reported up to now.

Early models were developed in the framework of 2D theory elasticity to explain the instability of nonhydrostatically stressed solids.[34,63] They established the criteria for films coherently attached to the rigid or isotopic deformable solid substrate along one of the two external boundaries. The basic mechanism considers that in the case of a nonplanar surface, stress is concentrated in the valleys and relieved on the mounds. Because the chemical potential is linearly proportional to the elastic energy density, the chemical potential is higher in the valley and lower on the mounds and thus atoms move from the valleys to the mounds tending to destabilize the surface. Capillarity has an opposite effect tending to stabilize the planar surface. This instability is independent of the sign of the applied stress. It was found[64] that the wave-number of the instability (q) varies as

$$q = \frac{2\pi}{\lambda} = \frac{\sigma^2 h}{\gamma\eta}(1-\nu),$$

where γ is the surface free energy, λ is the corrugation periodicity, σ is the misfit stress, η is the shear modulus, h is the deposited thickness, and ν is the Poisson coefficient. Following these classical models, λ should scale as $\gamma/\sigma^2 h$.[65,32]

On a vicinal substrate, considering the large density of steps, it has been shown that on strained layers there are long range attractive interactions between steps that are responsible for a step-bunching instability.[58] In contrast to con-

TABLE I. Evolution of rms roughness and $\lambda_\perp$ with the misorientation angle (θ) between 0.3 and 10° for $Si_{1-x}Ge_x$ layers with $x=0.35$ (misfit $m=\Delta a/a=1.46$) and $h=10$ nm.

Misorientation angle (°) from (001) to [110]	Terrace length (nm)	Correlation length $\lambda_\perp$ (nm)	rms (nm)
0.3	25.8	105	1.6
1	7.7	110	1.5
4	2	117	1.2
6	1.3	117	1.5
10	0.8	110	1.2

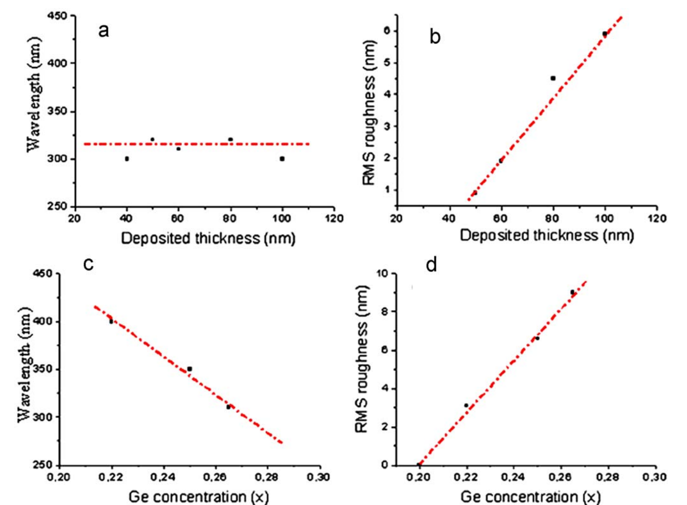

FIG. 5. (Color online) Morphological evolution of $Si_{1-x}Ge_x$ layers deposited on Si (001) 1.5° off. In the upper part is given the evolution with h (deposited thickness). In the lower part is given the evolution with x (Ge concentration). (a) and (c) give the evolution of the wavelength (λ) and (b) and (d) give the evolution of the rms roughness.

tinuum models, a step-bunching instability has no characteristic wavelength but proceeds by coalescence of step bunches following a time evolution of the characteristic bunch size: $\langle n \rangle \propto t^{1/6}$ with $\lambda = \langle n \rangle / \sin \theta$ (θ is the misorientation angle of the substrate). Following this model, the expected scaling of λ would be in $h^{1/6}$.

In fact, the theoretical treatment of the instability requires considering the mode of mass transport. In this framework, various processes such as bulk diffusion,[33] surface diffusion,[66,67] and evaporation-condensation[35] have been investigated. Moreover, stress dependent surface and interface mobility was also considered.[41,43] These models showed that the instability can be driven either by the stress dependent mobility or by the classical elastic energy. The first driving force gives an evolution of q in σ while the second driving force gives the classical evolution of q in σ^2. In the case of SiGe on Si(001) the stress dependent mobility term promotes the instability and should control the evolution of the morphology with a scaling of λ in σ^{-1}.

On the other hand a relevant effect is the alloy decomposition which is active during growth of strained layers, even for nominally stable alloys (consisting of atomic species of different size). In this situation, different diffusivities depending on the atomic species should be considered. They are generated by the inhomogeneous stress along the interface which tends to drive the large atoms in regions of more tensile stress and the small atoms in regions of more compressive stress. This compositional instability has been examined in the framework of continuum models. It was first shown that its effect is always stabilizing in step-flow growth mode regardless of the sign of the stress.[68] Recently, more complex coupling effects between solute strains (induced by composition variations in the alloy) and misfit strains were considered.[43,69] In the case of SiGe, Si atoms can be considered immobile with respect to Ge atoms, the model predicts a linear scaling of the wave number q with film composition ($\lambda \propto \sigma^{-1}$).[43] Such results are still controversial.[69]

The results on $Si_{1-x}Ge_x$ kinetic stress-driven instability reported above can be summarized as follows.

(1) On Si(111): kinetic stress driven instability is inhibited but step bunching develops on misoriented substrates.

(2) On Si(001): the ripples are not formed by a step bunching instability and they are not parallel to the substrate steps (on vicinal substrates, the ripples are even perpendicular to the substrate steps). Topographic evolution with h and σ differs on nominal and on vicinal substrates; on 1.5° off, the scaling of the amplitudes is $A \propto h$ and $A \propto \sigma$ and the scaling of the periodicity is $\lambda \propto h^0$ and $\lambda \propto \sigma^{-1}$.

All the experimental evolutions found are coherent with the models which consider strain dependent interface mobility (or solute stresses).[41,43] Regarding the effect of substrate orientation and misorientation, we suggest that the dependence of step energy and surface energy anisotropy on strain strongly affect the instability. This explains why the presence of steps on vicinal substrates considerably modifies the instability behavior by locally changing the stress relaxation and consequently the interfacial mobility. This also explains why the instability does not develop on Si(111).

In conclusion of this first part, we have investigated the self-organization processes of three different growth instabilities: step bunching, faceting, and kinetic stress-driven. Remarkably, in all the situations, full scale wafer patterns with specific topographic features and scalable amplitude, periodicity, and shape have been produced using a complex interplay of experimental parameters such as growth temperature, Ge concentration (x), deposited thickness (h), and misorientation angle (θ). Scaling evolutions of the different growth instabilities have been determined. Additionally to this systematic investigation it is possible to create specific patterning using predetermined experimental conditions.

B. Ge dots self-assembling

In this section, the aim is to understand the self-assembling processes of Ge dots on a prepatterned surface using a two step process. We first create full scale periodic nanopatterns by using one of the self-organization processes described above, then, we use these nanopatterns as a template for the subsequent ordering of Ge dots.

The effect of impurities and stress gradients (induced by misfit dislocations or by mesas) on Ge dots ordering has been evidenced already in the literature.[70,71] We focus in this section on the effect of surface steps and surface topography on the self-assembling process. It has already been shown in previous studies[72] that the ordering of Ge islands is not affected significantly by the monoatomic steps of the Si (001) substrate. Moreover, it was shown that during SiGe growth on vicinal Si(001) with a polar angle of 2° and an azimuthal angle of 45°, the step bunches formed during the early stage of strain relaxation guide the nucleation of {105} faceted islands.[73] However, the effect of a template layer with surface ripples was not clearly established. Step bunches were produced during the growth at 450 °C of Si on Si (001) 1.5° off substrate [Fig. 1(a)]. They self-organize into periodic wires with an aspect ratio $A/\lambda \sim 3 \times 10^{-3}$. On such a template layer, a preferential nucleation of Ge islands is expected along step bunches if the islands size is in the range of the ripples periodicity. The best ordering was obtained on a self-organized 500 nm thick Si template layer with step bunches 0.8 nm high and a 250 nm period. After the deposition of 8 ML Ge on this template, we can observe a preferential nucleation of domelike shaped Ge islands (~120 nm diameter and ~20 nm height) along the step bunches even if random nucleation is observed [Fig. 6(a)]. Higher magnification image [inset of Fig. 6(a)] evidences the position of Ge dots inside the valley between the ripples. These observations are confirmed by the 2DPSD of the surface before and after Ge deposition which shows similar periodicity with a slightly lower correlation length in the latter case due to random nucleation [Fig. 6(b)]. As a comparison the 2DPSD of the surface with Ge dots/unpatterned vicinal substrate is also plotted. We can clearly see that both the wavelength and the correlation length are very different from the patterned surface. This set of experiments proves that the nucleation barrier is lower along step bunches than on the (001) terraces, but is not low enough to prevent random nucleation which is facilitated by the low step edge energy on Si(001).

We then perform similar experiments on Si(111). We first create self-organized step bunches during deposition of Si on

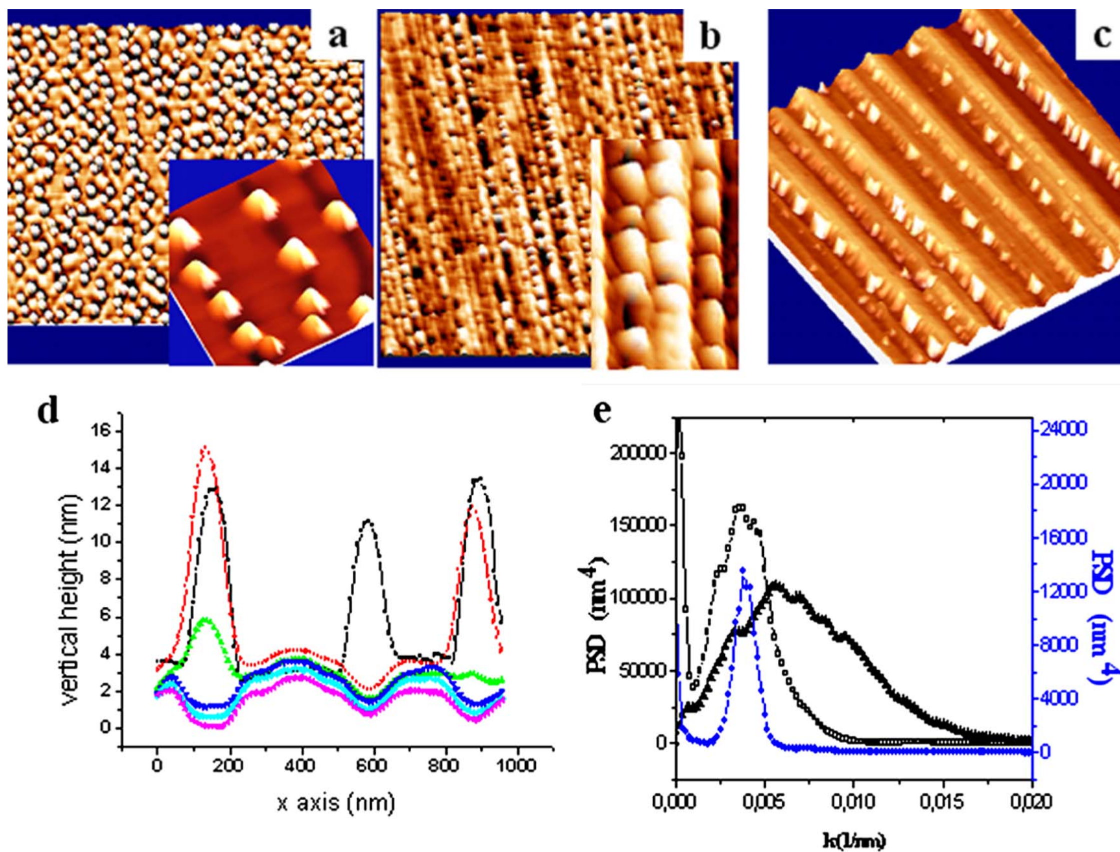

FIG. 6. (Color online) AFM images of the surface after growth of 8 ML Ge (T_g=600 °C)/500 nm Si on: (a) Si(001) 1.5° off (surface Fig. 1(a)); (b) Si(111) 1.5° off towards [11−2] (surface Fig. 2); (c) Si(111) 1.5° off towards [−1−12]. Scan size is 3×3 μm^2. (d) Succession of height profiles along the x axis of the inset of (a). Distance between line profiles is 20 nm. (e) Comparison of 2D power spectral density of the patterned substrate (circles); Ge dots deposited on patterned substrate (empty squares) and Ge dots deposited on unpatterned substrate (triangles).

Si(111) misoriented 1.5° towards [11−12] at 700 °C [Fig. 2(b)]. After deposition of 8 ML Ge on this template, we can see that almost all the islands grow along the (332) nanofacets [Fig. 6(c)]. A higher magnification image reveals the very nice alignment of typical triangular Ge islands [inset of Fig. 6(c)]. Such an alignment has already been reported in the literature.[72]

Deposition of 8 ML Ge on a self-organized step bunching instability (obtained during deposition of Si on Si(111) misoriented 1.5° towards [−1−12]) resulted in exactly the same situation with the alignment of triangular Ge islands along the step bunches [Fig. 6(c)]. This proves that both Si(111) nanofacets and step bunches represent very favorable sites of nucleation. Consequently the step bunches have a much larger influence on Ge dots nucleation on Si(111) than on Si(001). This could be attributed to the different surface energy anisotropy of Si(001) and Si(111) mainly induced by the different step edge energy.

We focus now on the combined effect of topography with strain gradients. For that, a SiGe strained layer with a square based periodic corrugation [obtained in the conditions described in Fig. 4(a) by deposition of 10 nm $Si_{0.75}Ge_{0.35}$ on vicinal Si(001) 1.5° off] is used as the template. During deposition of 8 ML Ge on this template, islands form and decorate the top of periodic mounds (and not the valley as in the previous case). At larger scale they order into 2D square arrays of dots with homogeneous size [Fig. 7(a)]. Large scale ordering of Ge dots on the template layer can be well-appreciated on 2DPSD of the template layer before and after Ge deposition [Fig. 7(b)], while almost no ordering is observed when islands are deposited on the unpatterned 1.5° off (001) substrate. In order to confirm the effect of the SiGe template on dots ordering, we have reproduced the experiment on a template layer obtained in the same experimental conditions on 10° off Si(001) [Fig. 4(b)]. Again, islands nucleate on the top of the undulations [Fig. 7(c)]. A remarkable ordering of Ge islands along the periodic linear undulations is produced as can be seen on the 2DPSD profiles [Fig. 7(d)] while again no ordering can be observed when the islands are formed on an unpatterned 10° off (001) substrate. In this situation the islands formed what were called “dome” islands.[74] Similar ordering has been reproduced with “hut” islands obtained at lower temperature (Fig. 8). In these two cases, the undulations are perpendicular to the initial train of steps of the substrate and the positioning of islands cannot be driven by the presence of underlying ML steps.

Let us summarize now the positioning of islands on the various self-organized instability patterns. It has been shown above that Ge dots grow inside the valley of the undulations in the absence of strain gradients (kinetic instability). They grow on the top of the undulations in the presence of strain

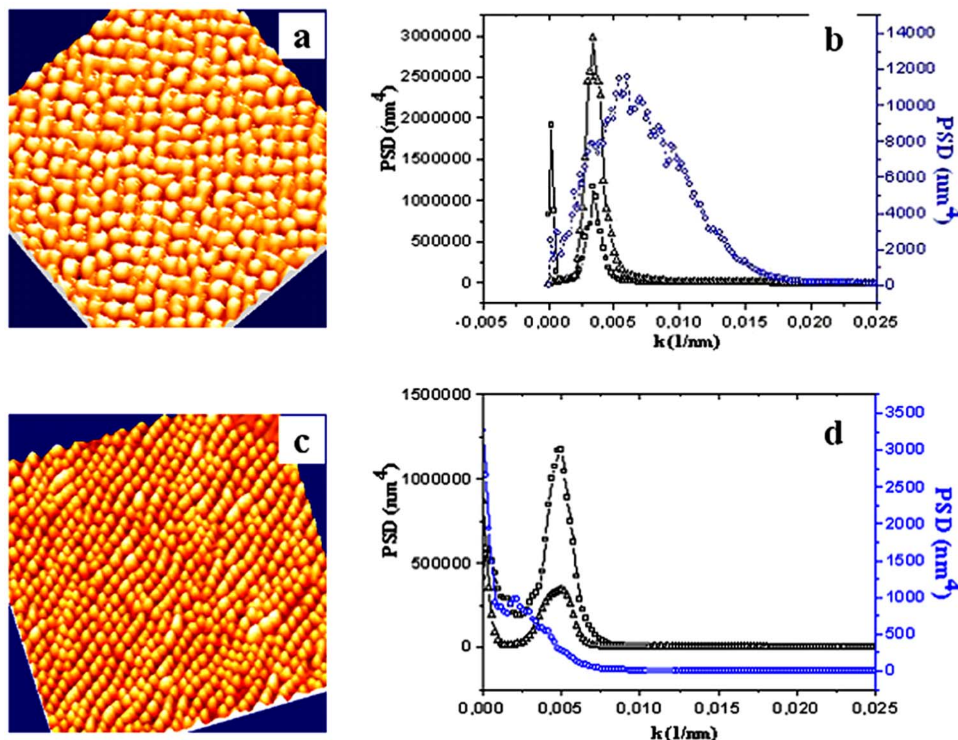

FIG. 7. (Color online) AFM images (left) and 2D PSD (right) of the surface after deposition of 8 ML Ge (T_g=600 °C) on $Si_{1-x}Ge_x$ template layer (h=10 nm and x=0.35) on (a) 1.5° off and (b) 10° off Si(001). Scan size is 5×5 μm^2. (c) and (d) give 2DPSD of (a) and (c) images, respectively. Comparison of 2DPSD before Ge deposition (triangles) and after Ge deposition on patterned (squares) and unpatterned substrate (circles) is given.

gradients (kinetic stress-driven instability). In our MBE growth conditions, nucleation of islands is controlled by the adatom velocity on the surface (V) which can be expressed as[35]

$$V = -\left(\frac{D_S}{kT}\right)\frac{\delta\mu}{\delta s},$$

where D_s is the coefficient of surface diffusion, $D_s = D_0 \exp(-E/k_B T)$, kT is the thermal energy, E is the activation energy of surface diffusion, and $\delta\mu/\delta s$ is the derivative of the chemical potential along the surface. On a corrugated substrate, E has two main components, the diffusion on terraces (E_T) and a contribution from the n nearest neighbors $(E_a): E = E_T + nE_a$. On step bunches due to the high density of steps, E is expected to be higher and D_s lower. As a consequence, kinetic driving force (and more precisely surface diffusion) should promote the nucleation of islands on step bunches and in the valley of the patterns.[75]

According to Ref. 76 the evolution of the chemical potential along the surface can be described by $\mu = \mu_0 + \Omega\gamma\kappa(x,y) + \Omega E_{el}(x,y)$ where the first term represents the surface free energy (γ) dependence with curvature $\kappa(x,y) = -h_{xx}(1+h_x^2)^{-3/2}$ and the second term represents the local elastic energy (E_{el}) and (Ω) is the atomic volume of the species. It is shown that the curvature dependent surface energy $\Omega\gamma\kappa(x,y)$ favors nucleation of islands on the concave parts (in the valley) while elastic energy $\Omega E_{el}(x,y)$ favors the nucleation on convex parts due to a reduction of the amount of compressive strain (on the top of the undulations).

As a consequence, we explain the preferential nucleation along step bunches, in the valley of the step-bunching instability observed experimentally on vicinal Si(111) by the dominant effect of surface diffusion. The decrease of surface diffusion in the bottom of the corrugation is expected to favor nucleation in this place. The low effect of step bunches on vicinal Si(001) could be attributed to the limited height extension of step bunches on Si(001) as compared to Si(111) (almost eight times higher). In the situation of islands growth

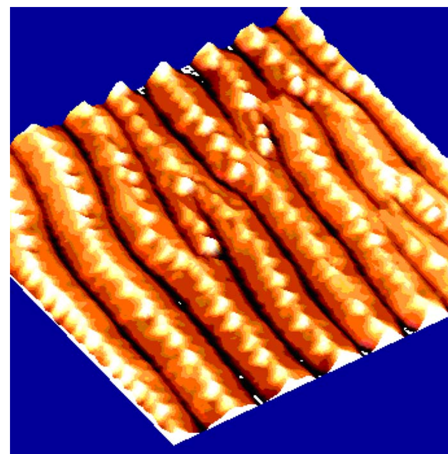

FIG. 8. (Color online) AFM image of the surface after deposition of 8 ML Ge (T_g=500 °C) on SiGe template layer (h=10 nm and x=0.35) on 10° off Si(001). Scan size is 1×1 μm^2.

on the faceting instability, the preferential nucleation at the intersection between facets in the valley can be attributed to the dominant effect of curvature dependent surface energy which favors nucleation on concave areas. Regarding islands growth on the stress-driven kinetic instability, the preferential nucleation on the top of the undulations can be explained by the dominant effect of a larger elastic strain relaxation on the top of the undulation which favors nucleation on these areas. Similar behavior was reported in the literature for Ge dots self-assembled on prepatterned substrates by means of lithographic tools.[76,77]

IV. CONCLUSION

In the first part, we have shown that self-organized growth instabilities can be used to create full scale wafer periodic nanopatterns which can serve efficiently as a template for Ge dots self-assembling. Step bunching and faceting instabilities which develop during the growth of Si on vicinal Si substrates, and stress-driven kinetic instability which develops during the growth of $Si_{1-x}Ge_x$ on vicinal Si(001) were investigated. Self-organization processes were determined as a function of temperature, deposited thickness, and strain. Morphological evolution of various instabilities has been addressed. In the second part, we have investigated the nucleation of Ge dots on self-organized template layers. We have shown that Ge dots preferentially nucleate on specific sites of the self-organized template layers, depending on the driving forces involved. In particular the preferential nucleation of Ge dots in the valley between step bunches is explained by a reduced surface diffusion while their position on the top of strained undulations is explained by elastic energy relaxation. Also, on a nanofaceted surface, the effect of surface energy anisotropy is the dominant driving force.

[1] C. Ratsch and A. Zangwill, Surf. Sci. **293**, 123 (1993).
[2] J. H. van der Merwe and E. Bauer, Phys. Rev. B **39**, 3632 (1989).
[3] D. J. Eaglesham and M. Cerullo, Phys. Rev. Lett. **64**, 1943 (1990).
[4] J. M. Baribeau, X. Wu, N. L. Rowell, and D. J. Lockwood, J. Phys.: Condens. Matter **18**, R139 (2006).
[5] B. Voigtlander, Surf. Sci. Rep. **43**, 127 (2001).
[6] J. Krug, V. Tonchev, S. Stoyanov, and A. Pimpinelli, Phys. Rev. B **71**, 045412 (2005).
[7] D. Kandel and J. D. Weeks, Phys. Rev. B **49**, 5554 (1994).
[8] T. Frisch and A. Verga, Phys. Rev. Lett. **94**, 226102 (2005).
[9] A. Pascale, I. Berbezier, A. Ronda, and A. Pimpinelli, Appl. Phys. Lett. **89**, 104108 (2006).
[10] M. Sato and M. Uwaha, Surf. Sci. **493**, 494 (2001).
[11] C. Schelling, G. Springholz, and F. Schäffler, Phys. Rev. Lett. **83**, 995 (1999).
[12] M. Rost, J. Krug, and P. Smilauer, Surf. Sci. **369**, 393 (1996).
[13] A. Ronda and I. Berbezier, Physica E (Amsterdam) **23**, 370 (2004).
[14] M. Siegert and M. Plischke, Phys. Rev. E **53**, 307 (1996).
[15] M. Sato and M. Uwaha, Phys. Rev. E **60**, 7120 (1999).
[16] M. Vladimirova, A. Pimpinelli, and A. Videcoq, J. Cryst. Growth **220**, 631 (2000).
[17] A. A. Golovin, M. S. Levine, T. V. Savina, and S. H. Davis, Phys. Rev. B **70**, 235342 (2004).
[18] F. K. Men, F. Liu, P. J. Wang, C. H. Chen, D. L. Cheng, J. L. Lin, and F. J. Himpsel, Phys. Rev. Lett. **88**, 096105 (2002).
[19] A. G. Cullis, MRS Bull. **21**, 21 (1996).
[20] D. E. Jesson, K. M. Chen, S. J. Pennycook, T. Thundat, and R. J. Warmack, Phys. Rev. Lett. **77**, 1330 (1996).
[21] P. Sutter and M. G. Lagally, Phys. Rev. Lett. **84**, 4637 (2000).
[22] R. M. Tromp, F. M. Ross, and M. C. Reuter, Phys. Rev. Lett. **84**, 4641 (2000).
[23] I. Berbezier, B. Gallas, A. Ronda, and J. Derrien, Surf. Sci. **412/413**, 415 (1998); I. Berbezier, B. Gallas, L. Lapena, J. Fernandez, and J. Derrien, and B. Joyce, J. Vac. Sci. Technol. B **16**, 1582 (1998).
[24] I. Berbezier, M. Abdallah, A. Ronda, A. Souifi, and G. Bremond, Mater. Sci. Eng., B **69-70**, 367 (2000).
[25] A. Ronda, M. Abdallah, J. M. Gay, J. Stettner, and I. Berbezier, Appl. Surf. Sci. **162-163**, 576 (2000).
[26] K. Sakamoto, H. Matsuhata, M. O. Tanner, D. Wang, and K. L. Wang, Thin Solid Films **321**, 55 (1998).
[27] J. Zhu, K. Brunner, and G. Abstreiter, Appl. Phys. Lett. **73**, 620 (1998).
[28] I. Berbezier, A. Ronda, A. Portavoce, and N. Motta, Appl. Phys. Lett. **83**, 4833 (2003).
[29] H. Omi and T. Ogino, Thin Solid Films **369**, 88 (2000).
[30] C. Teichert, J. C. Bean, and M. G. Lagally, Appl. Phys. A: Mater. Sci. Process. **67**, 675 (1998).
[31] J. J. Eggleston and P. W. Voorhees, Appl. Phys. Lett. **80**, 306 (2002).
[32] H. Gao, J. Mech. Phys. Solids **42**, 741 (1994).
[33] R. J. Asarro and W. A. Tiller, Metall. Trans. **3**, 1789 (1972).
[34] M. Grinfeld, Dokl. Akad. Nauk SSSR **290**, 1358 (1986).
[35] D. J. Srolovitz, Acta Metall. **37**, 621 (1989).
[36] A. Pidduck, D. Robbins, A. Cullis, W. Leong, and A. Pitt, Thin Solid Films **222**, 78 (1992).
[37] A. Oral and R. Ellialtioglu, Surf. Sci. **323**, 295 (1995).
[38] C. Duport, P. Nozières, and J. Villain, Phys. Rev. Lett. **74**, 134 (1995).
[39] F. Léonard and J. Tersoff, Appl. Phys. Lett. **83**, 72 (2003).
[40] I. Berbezier, A. Ronda, F. Volpi, and A. Portavoce, Surf. Sci. **531**, 231 (2003).
[41] W. Barvosa-Carter, M. J. Aziz, L. J. Gray, and T. Kaplan, Phys. Rev. Lett. **81**, 1445 (1998); J. F. Sage, W. Barvosa-Carter, and M. J. Aziz, Appl. Phys. Lett. **77**, 516 (2000).
[42] V. B. Shenoy, C. V. Ciobanu, and L. B. Freund, Appl. Phys. Lett. **81**, 364 (2002).
[43] B. J. Spencer, P. W. Voorhees, and J. Tersoff, Phys. Rev. B **64**, 235318 (2001).
[44] B. Voigtlander, T. Weber, P. Smilauer, and D. E. Wolf, Phys. Rev. Lett. **78**, 2164 (1997).
[45] N. Motta, J. Phys.: Condens. Matter **14**, 8353 (2002).
[46] P. Sutter, I. Schick, W. Ernst, and E. Sutter, Phys. Rev. Lett. **91**, 176102 (2003).

[47] V. B. Shenoy and L. B. Freund, J. Mech. Phys. Solids **50**, 1817 (2002).
[48] J. Tersoff, B. J. Spencer, A. Rastelli, and H. von Känel, Phys. Rev. Lett. **89**, 196104 (2002).
[49] P. Sutter, E. Sutter, and L. Vescan, Appl. Phys. Lett. **87**, 161916 (2005).
[50] L. Vescan and T. Stoica, J. Appl. Phys. **91**, 10119 (2002).
[51] C. Teichert, C. Hofer, K. Lyutovich, M. Bauer, and E. Kasper, Thin Solid Films **380**, 25 (2000).
[52] I. Berbezier, A. Ronda, and A. Portavoce, J. Phys.: Condens. Matter **14**, 8283 (2002).
[53] R. J. Phaneuf, E. D. Williams, and N. C. Bartelt, Phys. Rev. B **38**, 1984 (1988).
[54] R. J. Phaneuf, N. C. Bartelt, Ellen D. Williams, W. Świech, and E. Bauer, Phys. Rev. Lett. **67**, 2986 (1991).
[55] J. Viernow, J.-L. Lin, D. Y. Petrovykh, F. M. Leibsle, F. K. Men, and F. J. Himpsel, Appl. Phys. Lett. **72**, 948 (1998).
[56] J. B. Hannon, J. Tersoff, and R. M. Tersoff, J. Cryst. Growth **237-239**, 181 (2002).
[57] P. D. Szkutnik, A. Sgarlata, A. Balzarotti, N. Motta, A. Ronda, and I. Berbezier, Phys. Rev. B **75**, 033305 (2007).
[58] J. Tersoff, Y. H. Phang, Z. Zhang, and M. G. Lagally, Phys. Rev. Lett. **75**, 2730 (1995).
[59] P. Raiteri, D. B. Migas, L. Miglio, A. Rastelli, and H. von Känel, Phys. Rev. Lett. **88**, 256103 (2002).
[60] Y. Fujikawa, K. Akiyama, T. Nagao, T. Sakurai, M. G. Lagally, T. Hashimoto, Y. Morikawa, and K. Terakura, Phys. Rev. Lett. **88**, 176101 (2002).
[61] A. Ramasubramaniam and V. B. Shenoy, J. Appl. Phys. **95**, 7813 (2004).
[62] A. Pascale, I. Berbezier, A. Ronda, and P. Kelires (unpublished).
[63] M. A. Grinfeld, Sov. Phys. Dokl. **31**, 831 (1986).
[64] M. A. Grinfeld, J. Intell. Mater. Syst. Struct. **4**, 76 (1993).
[65] W. H. Yang and D. J. Srolovitz, Phys. Rev. Lett. **71**, 1593 (1993).
[66] B. J. Spencer, P. W. Voorhees, and S. H. Davis, Phys. Rev. Lett. **67**, 3696 (1991).
[67] B. J. Spencer and D. I. Meiron, Acta Metall. Mater. **42**, 3629 (1994).
[68] J. Tersoff, Phys. Rev. Lett. **77**, 2017 (1996).
[69] Z. F. Huang and R. C. Desai, Phys. Rev. B **65**, 205419 (2002).
[70] C. Teichert, Phys. Rep. **365**, 335 (2002).
[71] A. Portavoce, I. Berbezier, and A. Ronda, Phys. Rev. B **69**, 155416 (2004).
[72] A. Sgarlata, P. D. Szkutnik, A. Balzarotti, N. Motta, and F. Rosei, Appl. Phys. Lett. **83**, 4002 (2003).
[73] C. Teichert, Phys. Rep. **365**, 335 (2002).
[74] It has been shown that depending on the growth conditions, either “hut” islands with pyramidal shape or “dome” islands with rounded shape can be formed. The shape transition between “hut” and “domes” islands has been explained by stress relaxation (Ref. 52). An extensive description of Ge islands can be found in Ref. 73.
[75] L. Nurminen, A. Kuronen, and K. Kaski, Phys. Rev. B **63**, 035407 (2000).
[76] M. Borgström, V. Zela, and W. Seifert, Nanotechnology **14**, 264 (2003).
[77] A. Karmous, A. Cuenat, A. Ronda, I. Berbezier, S. Atha, and R. Hull, Appl. Phys. Lett. **85**, 6401 (2004).